Turbulent transport at the thermal internal boundary-layer top: wavelet analysis of aircraft measurements

Stefano Galmarini, Jean-Luc Attié

TURBULENT TRANSPORT AT THE THERMAL INTERNAL BOUNDARY-LAYER TOP: WAVELET ANALYSIS OF AIRCRAFT MEASUREMENTS

S. GALMARINI*
Environment Institute, Joint Research Center, Ispra, Italy

J. L. ATTIÉ
Laboratoire d'Aérologie, UMR CNRS-UPS 5560, Toulouse, France

Abstract. Aircraft measurements of turbulent fluxes of scalars collected during the *BEMA* campaign at the Mediterranean Spanish coast have been analysed using wavelet techniques. The analysis aims at characterising the boundary-layer structure present during a period of the campaign with particular attention to the role of the Thermal Internal Boundary Layer (TIBL) in regulating the exchange processes with the overlying free atmosphere. The analysis of the data obtained by flying through the turbulent layer reveals the presence of characteristic structures as the aircraft crosses the TIBL top. These occur in a specific space and scale range. Comparisons of the result of the analysis obtained for different types of scalars give evidence that the region corresponding to the detected scales can be identified with the entrainment zone of the TIBL.

Keywords: TIBL, Entrainment, Aircraft measurements, Wavelet analysis.

1. Introduction

The Thermal Internal Boundary Layer (TIBL) is the atmospheric turbulent layer often found in coastal regions. In particular this layer forms in the presence of an advective flow driven by mesoscale processes (e.g., sea or lake breezes) through a discontinuity in roughness, temperature, heat and moisture flux, such as a water-land interface. In contrast to the so-called Internal Boundary Layer (IBL), the TIBL is characterised by the presence of the above mentioned elements and a well-defined temperature stratification. For a complete review see Garratt (1990).

As shown in the past by several authors (e.g., Raynor et al., 1975; Weisman, 1976; Simpson et al., 1980; Vugts and Businger, 1977; Venkatram, 1977; Smedman and Hogstrom, 1983; Stunder and Sethuraman, 1985; Ohara and Ogawa, 1985; Venkatram, 1986; Oke, 1987; van Dop et al., 1979) the TIBL structure and characteristics have a considerable relevance as far as turbulent transport is concerned. Under a sea-breeze regime for example, the internal turbulent state of the layer controls the entrainment of overlying air and its fumigation down to the surface.

* Corresponding author address: Stefano Galmarini, T.P. 321, Environment Institute, Joint Research Center Ispra, 21020, Ispra (Va), Italy. E-mail: stefano.galmarini@jrc.it

Conversely the formation of an IBL over the water surface (Garratt, 1992) can lead to the storage of pollutants emitted over land that can be re-advected on shore the following day.

An important part of any boundary-layer archetype is the Entrainment Zone (EZ) i.e., the part of the layer that interfaces with the overlying atmosphere (Tennekes, 1974). Through this part of the layer, fundamental for boundary-layer development and growth, heat and mass are exchanged. While the EZ of the horizontally homogeneous convective boundary layer (CBL) has been widely studied in the past by means of field campaigns, laboratory experiments and numerical models, little is known about it as far as the TIBL is concerned. Most of the modelling approaches assume an analogy between the EZ of the horizontally homogeneous convective boundary layer and that of the TIBL to derive parameters such as the TIBL depth (e.g., Steyn and Oke, 1982; Druilhet et al., 1997).

In this study the turbulent structure of the TIBL that develops over the eastern coast of Spain is investigated using the aircraft measurements collected during the Biogenic Emission over the Mediterranean Area (*BEMA*) campaign at Burriana. Particular care is paid to the TIBL structure under stationary conditions, i.e. when the sea-breeze flow is well established. To determine the TIBL structure, mean meteorological variables are used together with direct measurements of turbulent quantities. The use of wavelet analysis allows us to: recognize the EZ of the layer; determine the fluxes that control the turbulent exchange between the TIBL top and the overlying atmosphere; identify the turbulent scales that characterise the turbulent exchange.

2. The Aircraft Campaign during *BEMA* at Burriana

The *BEMA* experiment aimed at identifying the role of biogenic emissions on tropospheric ozone production. During the period from 1994 to 1997, a series of extensive campaigns were conducted in different coastal regions of the Mediterranean basin (Seufert, 1997). Among them, in June 1997 a campaign took place near the coast of Spain, north of Valencia (Figure 1), selected, among other reasons, for the intensive agricultural and industrial activities and thus for the presence of large biogenic and anthropogenic emissions. The French research aircraft ARAT (Avion de Recherches Atmosphériques et de Télédétection, Durand et al., 1989; Lambert and Durand, 1998) was used to collect mean meteorological and turbulence measurements in addition to concentrations of reactive tracers. The aircraft travels at an average speed of about 80 m s^{-1} and it is equipped with several types of probes. Table I summarises the variables measured on board and used in this study, the equipment adopted and the sampling rate. The flight plan consisted of two to three flights daily, mainly in the early and central hours of the day, for a total number of five days between 9 and 13 June 1997. In this study we concentrate on the flights conducted on June 12 and 13. During these days a high pressure

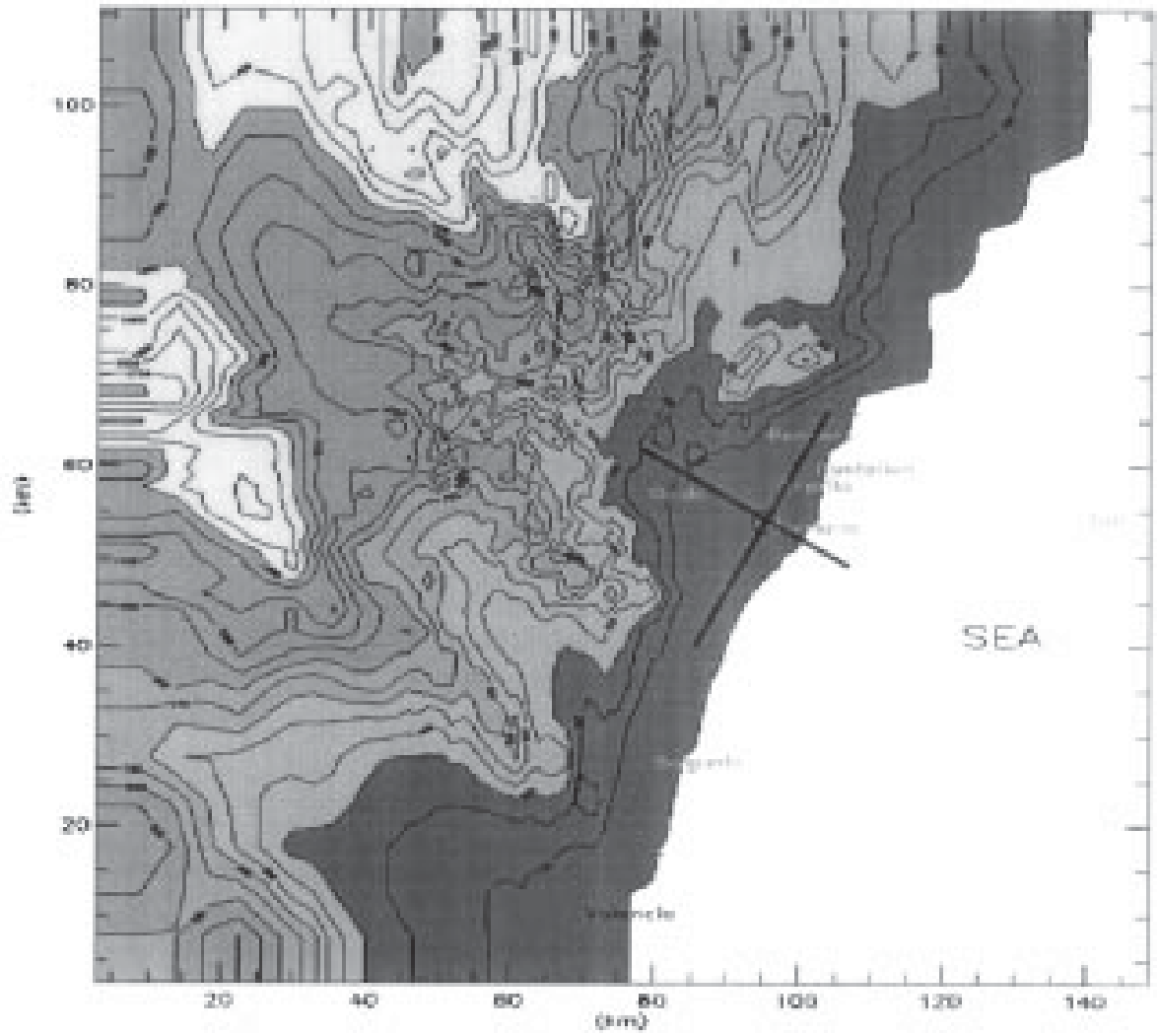

Figure 1. Map of the topography of the Eastern coast of Spain where the campaign took place. The two lines indicate the transects of the aircraft perpendicular and parallel to the coast.

system developed over the Mediterranean generating a weak geostrophic flow onto the Iberian peninsula and a well-established sea-breeze regime on its eastern coast. High to middle level clouds where present in the region with no associated precipitation. Flight legs perpendicular and parallel to the coast line were conducted at different levels with profiles collected at specific locations. The legs perpendicular to the coast started over the sea and crossed the coast over the Burriana urban settlement (Figure 1). The analysis presented here will focus only on the data collected during these flights since a large spatial heterogeneity is present as far as the coastal orographic features and land use are concerned.

TABLE I

Variables measured on the ARAT during BEMA and used in this study.

	Instrument	Sampling frequency (s^{-1})
Wind speed	INS Sagem ULIS 45I; Radome	64; 64
Temperature	Rosemount 102 E2-AL	64
Moisture	Lyman-α AIR LA1; Dewpoint temp. General Eastern	256; 8
Ozone mean conc.	Thermo-Electron, Environment S.A.	4
Ozone conc. fluct.	OSG2	64

3. TIBL Structure on 12 and 13 June 1997

3.1. Mean structure

Figures 2a–c show the vertical profiles of wind vector, potential temperature, moisture and ozone concentration collected on June 12 at three points (D, C, SEA) located on the line perpendicular to the coast, crossing the site of Burriana and covering a horizontal distance of 45 km. The vertical profiles of the four variables show that a clear sea-breeze flow is present from the surface (sea and land) up to approximately 1000 m while an off-shore flow is active in the upper layers. The measured wind shows also the presence of a layer between the sea breeze and the return flow where the wind is directed through the plane, i.e., northward along the coast.

From the temperature profiles the position of the temperature inversion at the three locations can be evinced. One can notice that moving from point SEA to point D the inversion is located at higher levels. The moisture vertical distribution shows a sudden variation at the temperature inversion. Below this point it is well distributed in the vertical over the sea and the land. The ozone profile shows also a clear structure. Several concentration maxima are visible in the vertical. Over the sea and the land, ozone is distributed relatively homogeneously in the vertical up to the temperature inversion level.

A similar vertical structure is found on June 13 as shown in Figure 3a–c. On 13 June the wind is significantly stronger than the day before throughout the domain. In this case, the breeze flow, the temperature inversion and the ozone maxima are even clearer than on June 12. Moisture is clearly well mixed at SEA and C with a sudden reduction in mixing ratio at the temperature inversion level, whereas in D a rather constant decrease with height is present. Ozone appears well mixed in the vertical at D and decreases rapidly as the profile approaches the surface at C.

The information extracted from the vertical profiles of mean meteorological variables is summarised in the sketch of Figure 4. The simplified structure of Figure

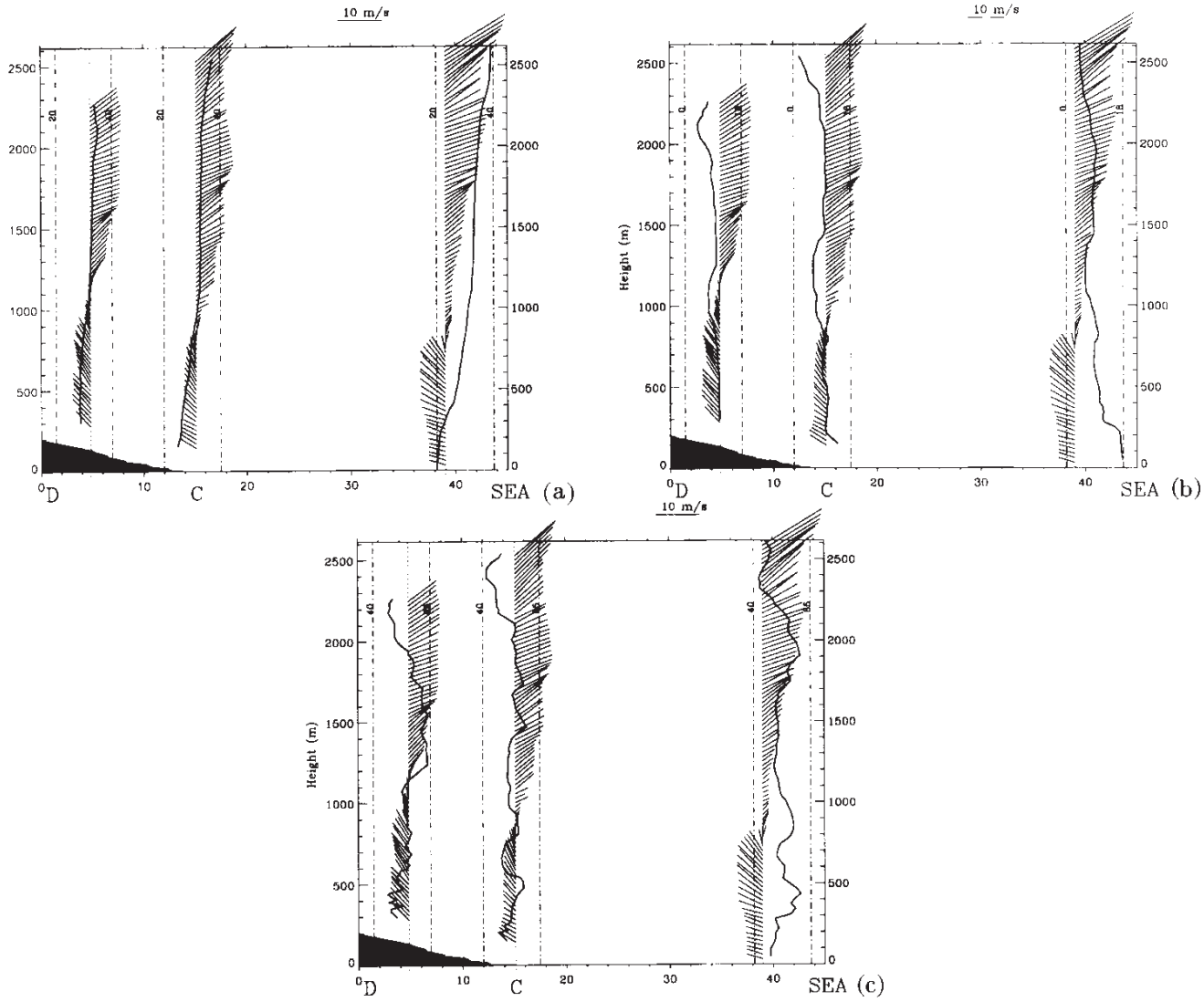

Figure 2. Profiles of wind, moisture, potential temperature and ozone on June 12 1997 at noon. (a) Potential temperature (range in degrees Celsius along the dashed line) and wind vectors; (b) Moisture (range in g kg^{-1} along the vertical dashed line) and wind vectors; (c) Ozone concentration (indicated in ppb along the vertical dashed lines) and wind vectors.

4 has been slightly exaggerated to emphasise the main features deduced from the data. In the figure we have identified:

- a Breeze Flow Layer (BFL): developing from the sea (land) surface to approximately 900 m (point D) in which the flow is directed inland;
- a Shear Flow Layer (SFL): extending for few hundreds of metres in the vertical and in which the wind is directed northward along the coast;
- a Return Flow Layer (RFL): where the sea-breeze return flow is directed toward the sea.

This layer structure seems to be a general feature of this region since it was also observed during the MECAPIP campaign as reported by Millan et al. (1992). The temperature inversion and the moisture distribution (not shown in the figure) have been used to derive the boundary-layer depth. A shallow neutrally-stratified mixed layer, approximately 100 m deep, is identified over the sea and a TIBL develops over the coast up to 900 m on the 12th and approximately 700 m on the 13th. As shown later, the data collected do not provide clear information on the TIBL

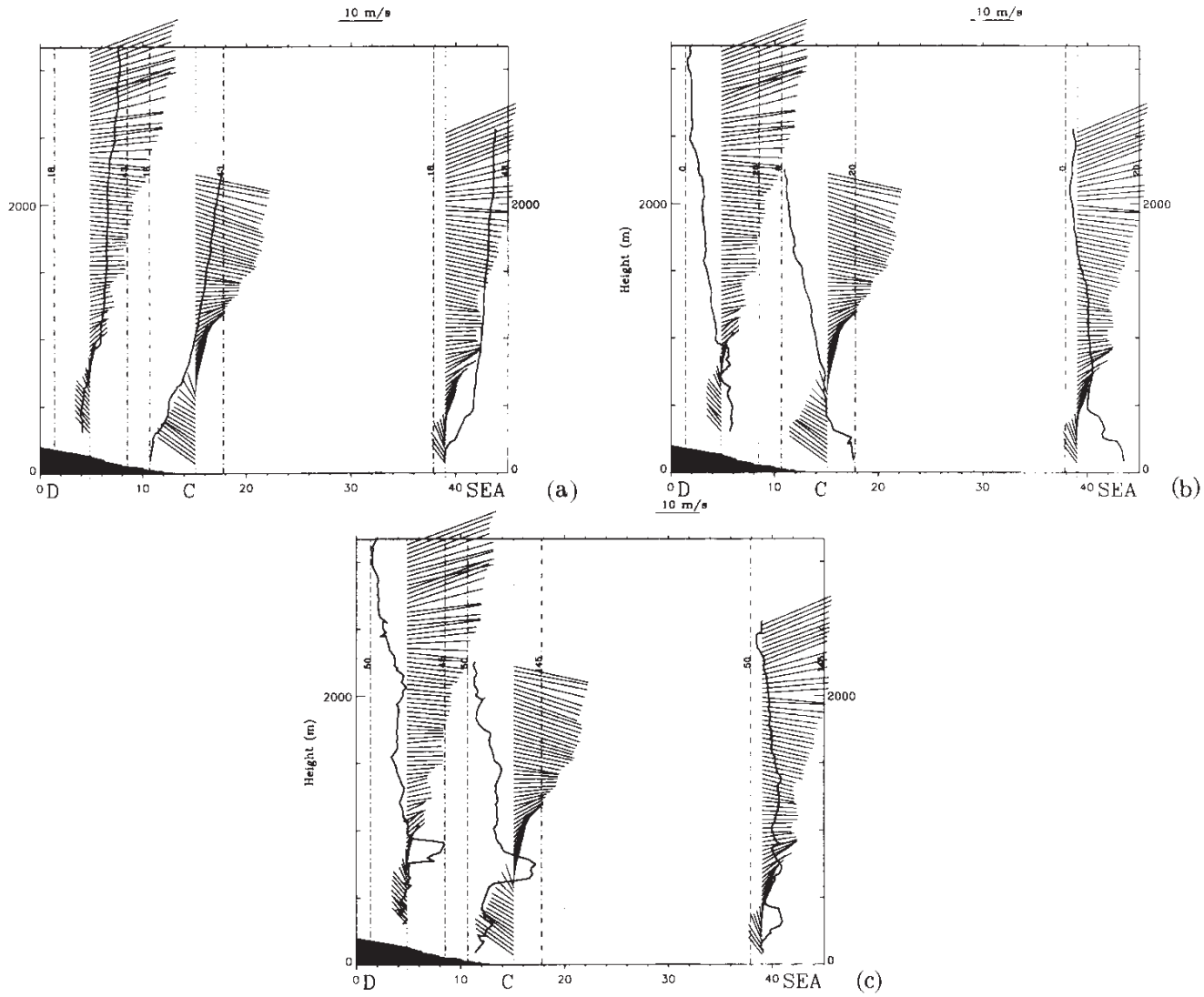

Figure 3. Profiles of ozone, wind and potential temperature on June 13 1997 at noon. (a) Potential temperature (range in degrees Celsius along the dashed line) and wind vectors; (b) Moisture (range in g kg^{-1} along the vertical dashed line) and wind vectors; (c) Ozone concentration (indicated in ppb along the vertical dashed lines) and wind vectors.

structure close to the shore line. It appears as if an almost continuous transition is present between the Marine Boundary Layer (MBL) and the TIBL. The vertical profiles of mean ozone concentration match quite well with the overall structure. For both the 12th and 13th, each of the layers contains an ozone maximum. The only exception is the shallow boundary layer over the sea and what we have recognised as the TIBL. In the latter, ozone is either decreasing sharply with height (as in the coastal region on both days) or is homogeneously distributed in the vertical indicating well-mixed conditions. The maximum of ozone concentration present in the RFL can be attributed to the photochemical production over land on the previous day, which has been accumulating in the reservoir layer. The origin of the maximum in the SFL is difficult to determine. The wind direction along the coast might indicate that ozone has been produced along the south coast and is being transported northward by the mean flow. The sharp reduction of ozone at the coast could be attributed to photochemical depletion due to the presence on the coast of

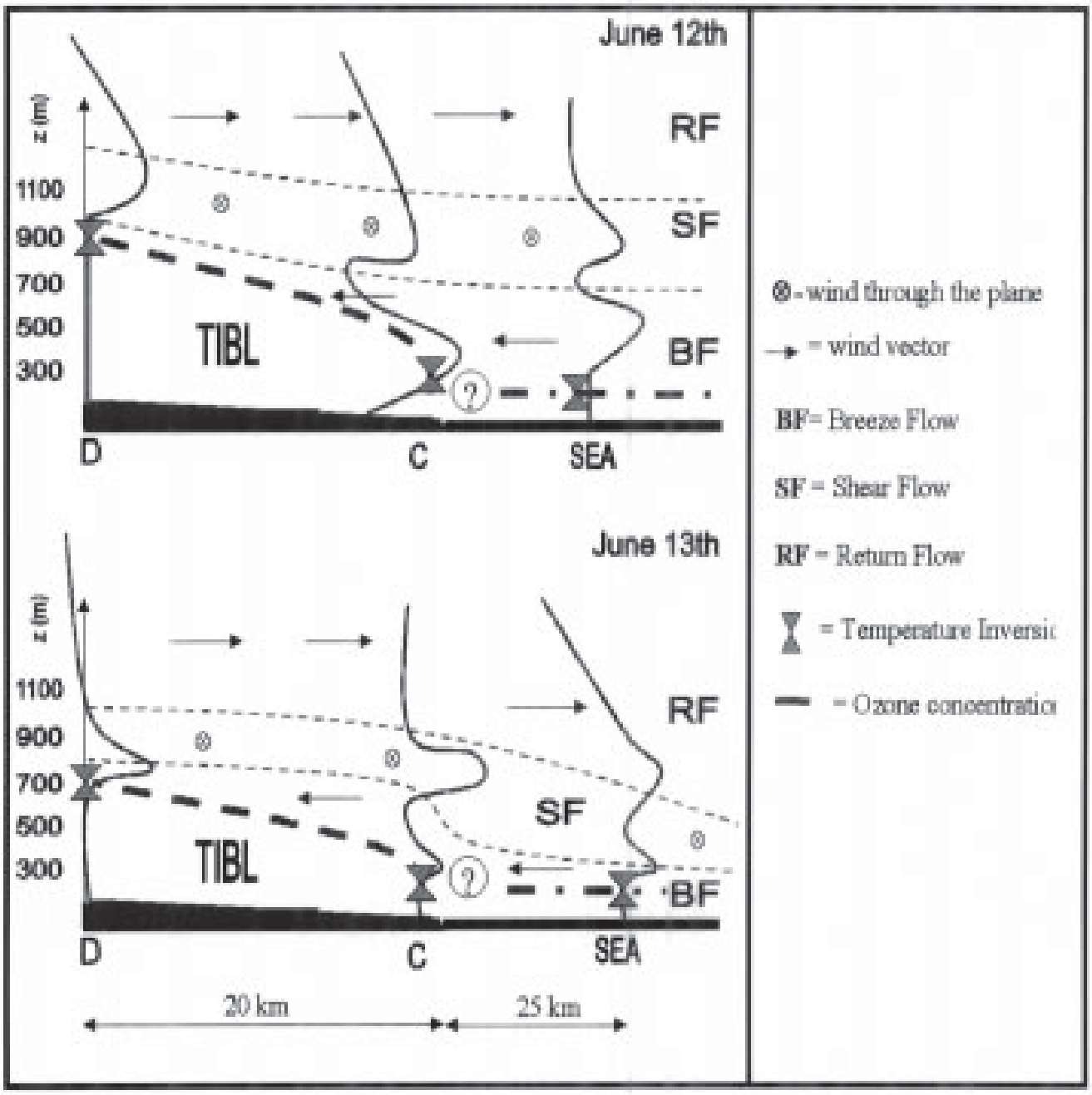

Figure 4. A sketch deduced from the mean measurements of wind direction, temperature and ozone concentration reconstructed to summarise the overall atmospheric vertical structure on the 12 and 13 June at noon in the plane perpendicular to the coast. The sketch has been obtained by analysing the profiles collected by ARAT at locations C, D and SEA.

urban settlements. However this aspect goes beyond the scope of this study and ozone will mainly be treated as a tracer.

3.2. Turbulent fluxes and variances

As mentioned above, during the ARAT flights direct measurements of turbulent variables were collected. Figures 5a–d give contours of the turbulent kinetic energy, sensible heat flux, ozone flux and the latent heat flux (respectively) on the 12th. In the figure, only the portion of the leg over land is shown (between point C and point D). The leg is indicated in the figure by the dashed line. The horizontal flights were

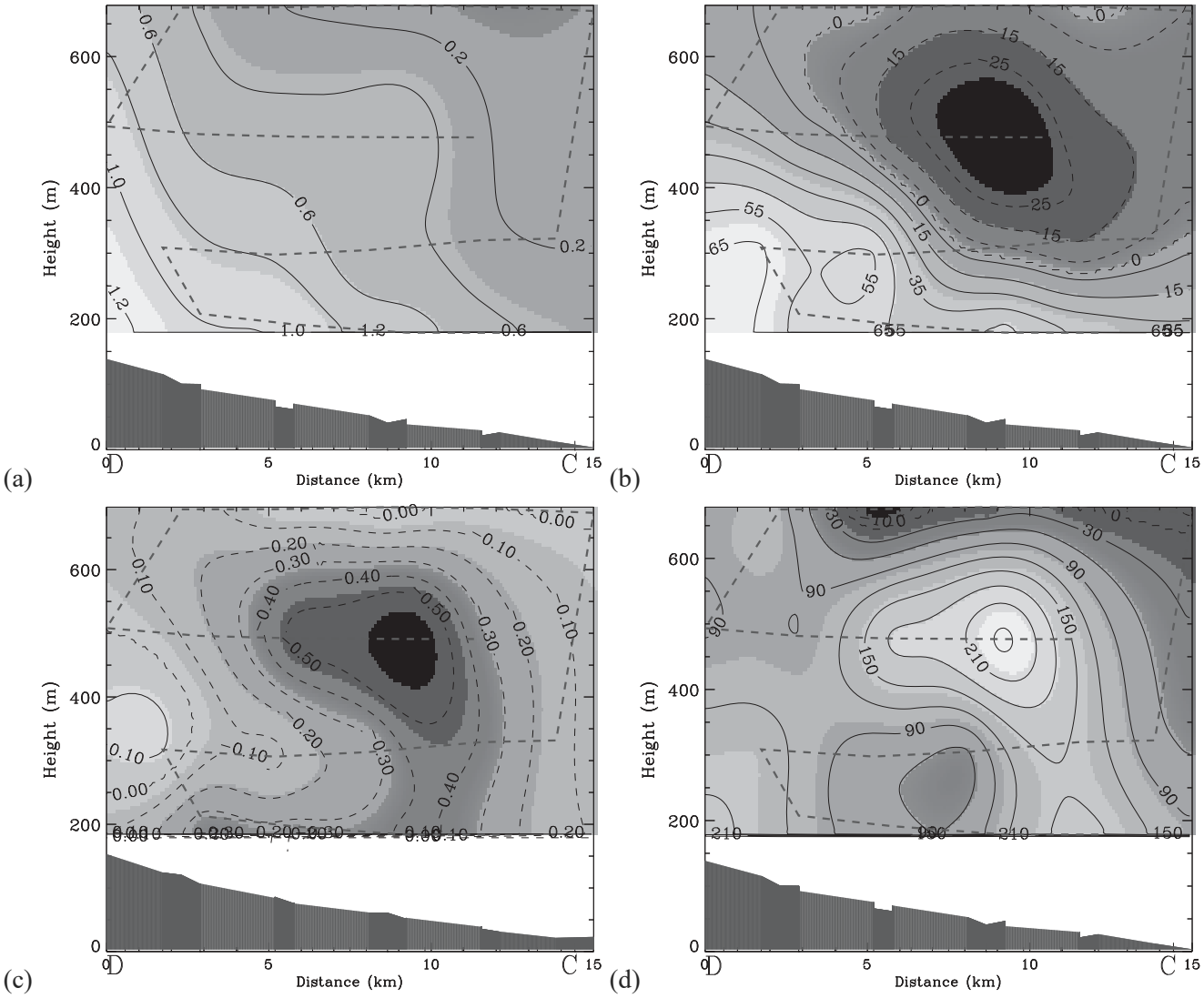

Figure 5. Noon flight perpendicular to the coast on June 12 1997. (a) TKE (m^2 s^{-2}); (b) Sensible heat flux (W m^{-2}); (c) Ozone flux (ppb m s^{-1}); and (d) Latent heat flux (W m^{-2}). The horizontal dashed lines represent the flight leg.

conducted at 180, 300, 480 and 680 m, the height of the flight leg is referred to mean sea level (m.s.l.), the terrain elevation detected by the aircraft is indicated at the bottom of each frame. The interpolation procedure is a standard method based on an approximation generating a minimum curvature solution.

Figure 5a shows the measured turbulence intensity (TKE) and thus the extent of the TIBL. The distribution pattern is in good agreement with the sketch obtained from the mean variables, given on one hand the reconstruction of Figure 5 on the basis of three vertical profiles and on the other hand the fact that an interpolation has been adopted to produce Figure 5. High TKE values are detected as the leg approaches point D partly due to the fact that there the aircraft reached the minimum distance from the surface.

Both sensible heat and ozone fluxes (Figures 5b and c) show negative values at the TIBL top confirming the results obtained from the mean profiles. The kinematic heat flux distribution show a clear square-root of distance dependence, an exception being the area around point C. A structure similar to that presented in Figure 5b

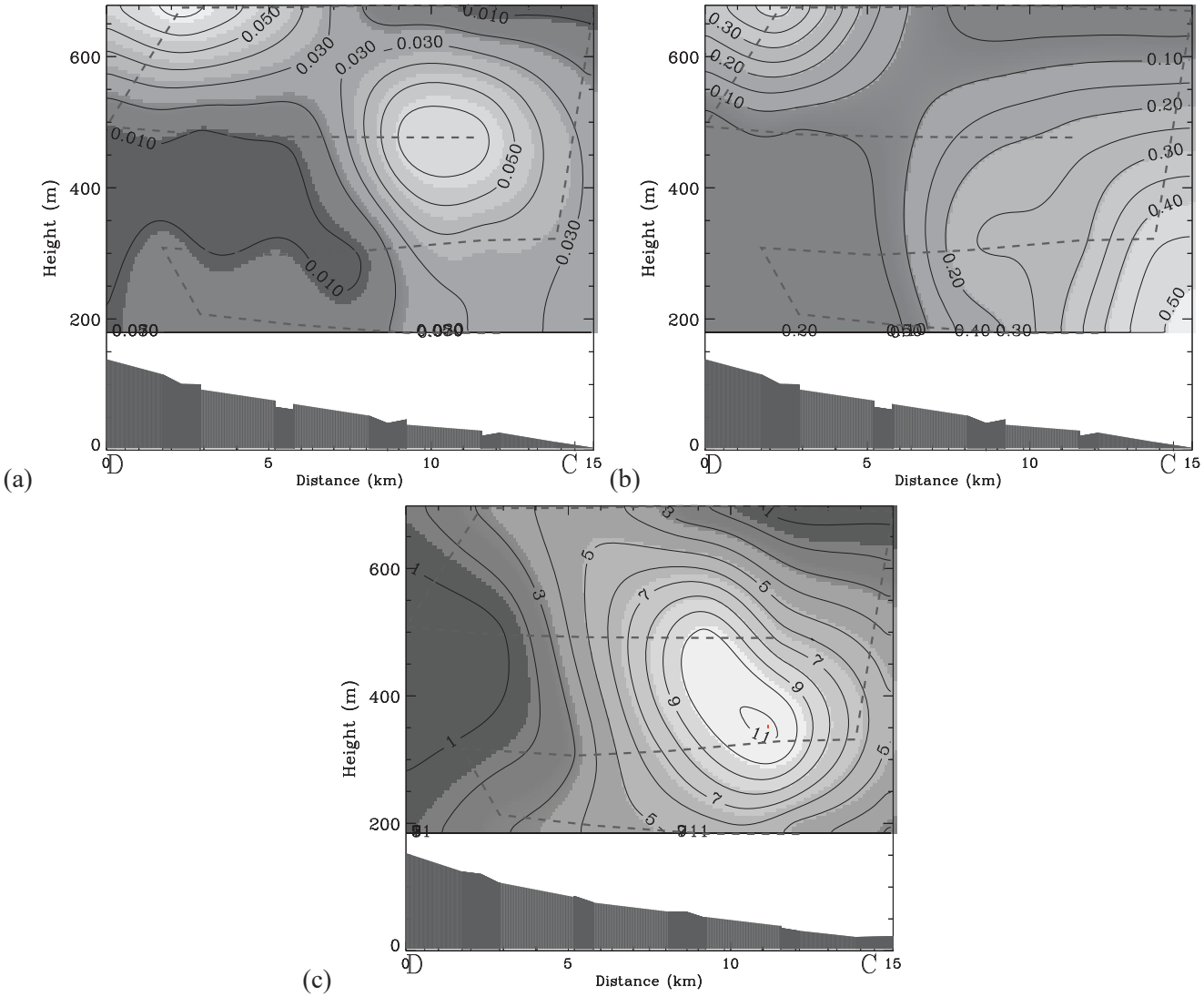

Figure 6. Noon flight perpendicular to the coast on 12 June 1997. (a) Temperature variance (K^2); (b) moisture variance ($g^2\ kg^{-2}$); (c) ozone variance (ppb^2). The horizontal dashed lines represent the flight leg.

was detected during the COAST experiment as presented by Durand et al. (1989). A large plume of ozone moving towards the surface can be recognised in Figure 5c. An area of large latent heat flux (Figure 5d) is found to correspond with the negative heat flux region.

The potential temperature variance ($\overline{\theta'^2}$) is plotted in Figure 6a and shows a maximum at the level where we have identified the TIBL top from the temperature profile. A similar pattern is given by the moisture variance ($\overline{q'^2}$) (Figure 6b). In this case a maximum is found close to ground level on the coast, probably due to moisture advection from the sea. The ozone variance ($\overline{O_3'^2}$) is presented in Figure 6c. Even in this case the turbulent quantity shows a maximum at the TIBL top though extending within the TIBL and following very closely the ozone flux distribution shown earlier. The maximum is also confined to the first middle part of the domain flown by the aircraft. The presence of variance maxima at the TIBL top, also typical of the CBL, agrees well with the results of Durand et al. (1989), though present in this case in a more blotchy distribution.

Turbulent flux and variance distributions similar to those of the 12th are found for 13 June.

In order to provide a better picture of the turbulent fluxes along the flight and to avoid misleading information introduced by the interpolation procedure, we show in Figure 7 the raw turbulence data. For simplicity, the figure shows only the product $w'\theta'$ at each level flown on June 12 at noon in the plane perpendicular to the coast; the other variables show a similar behaviour. The flight legs at 300 and 480 m show a clear sudden variation of the value of $w'\theta'$ indicating the exact location of the airplane transition from the BFL to the TIBL. This is also clear at 680 m although the intensity of the fluctuation is much smaller. At 180 m, the transition is not so clear, as if the aircraft has entered the TIBL already. Over the sea, $w'\theta'$ is very small and regular though slightly increasing as the leg approaches the coast. The behaviour found at 180 m and over the sea, indicates a TIBL starting off-shore or smoothly merging with the MBL. The values of $\rho c_p \overline{w'\theta'}$ obtained by overlapping averages of $w'\theta'$, are given by the dot-dashed line. The sensible heat flux obtained at 300, 480 m and 680 m shows a clear negative value right after the passage to the TIBL. At 180 m, the sensible heat flux is always positive and reduces to small values in the vicinity of the coast line.

From the results of Figure 7 we may conclude that the transition from the BFL and the TIBL are characterised by a clear entrainment process (namely of heat in the case of Figure 7) and that at small distances from the surface the TIBL seems to be already present a few kilometres off-shore.

4. Characterisation of the Turbulence Structure by Wavelet Analysis

To get more insight in the turbulence characteristics of the TIBL, a wavelet analysis has been conducted on the data sets. In particular we have focused on the vertical fluxes of temperature, moisture and ozone.

As mentioned by Druilhet and Durand (1997), wavelet analysis provide three main advantages compared to classical Fourier analysis: it allows the identification of isolated (in time and/or space) events; it provides their spectral structure; and it places events in precise locations and times. Wavelet analysis is thus an appropriate tool for studying inhomogeneous signals such as those considered in this study.

Given a series of data x_n for $n = 1, \ldots, N$ the wavelet transform reads:

$$W_n^x(s) = \sum_{k=0}^{N-1} \hat{x}_k \hat{\psi}^*(s\omega_k) e^{i\omega_k n \delta t} \tag{1}$$

where s is the wavelet scale, δt the data spacing and $\hat{x}_k$ is the discrete Fourier transform of x_n. In expression (1), $\hat{\psi}^*(s\omega_k)$ is the complex conjugate of the Fourier transform of the mother function ψ, which in this study is the well-known Morlet mother function (Grossman and Morlet, 1984).

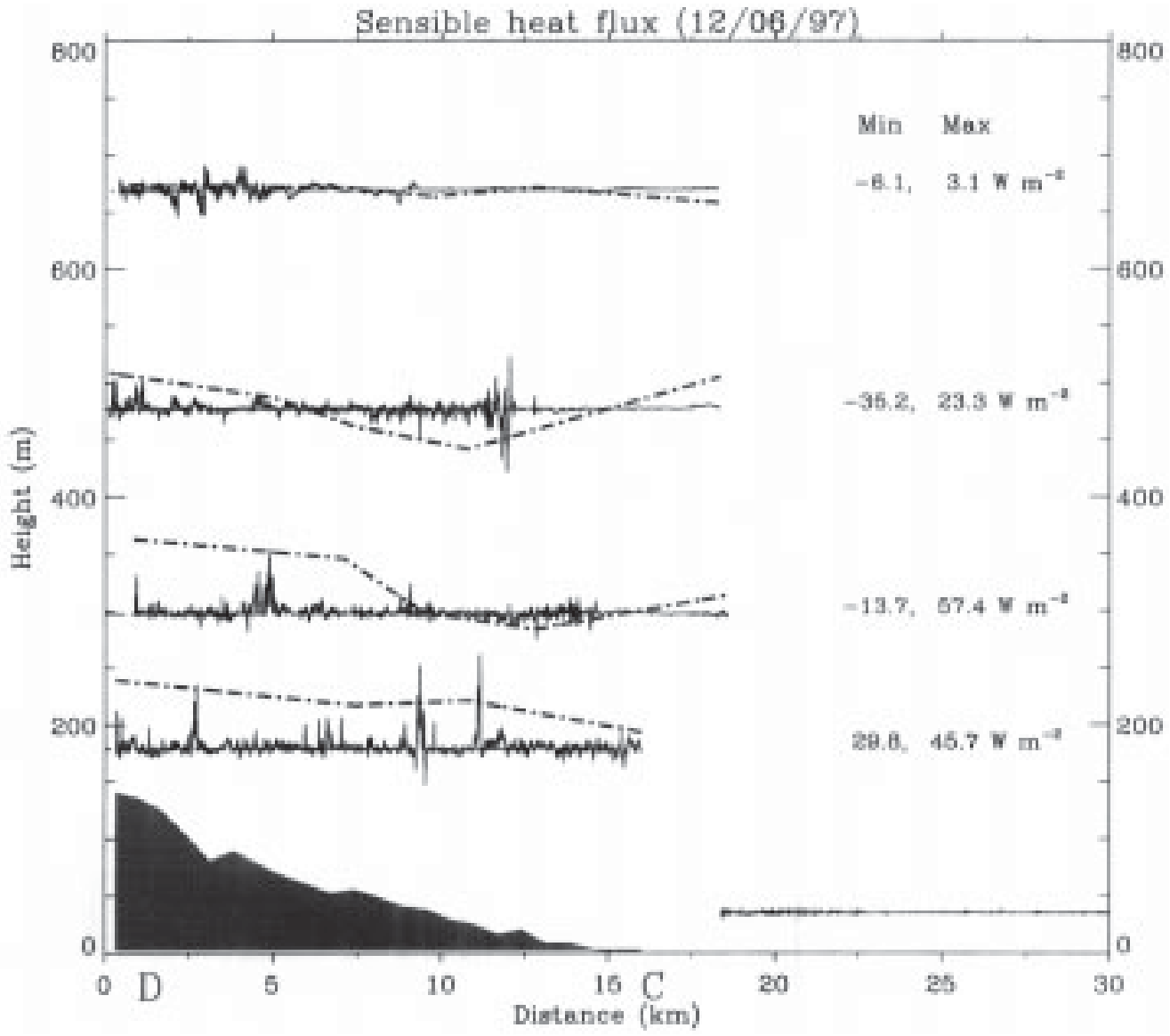

Figure 7. Noon flight perpendicular to the coast on June 12 1997. Raw data of $\rho c_p w'\theta'$ at the various measuring levels. The dot-dashed line is the averaged value flux. The figures on the right give minimum and maximum value in Wm^{-2} at each level.

The Fourier transform of the mother function appearing in (1) reads:

$$\hat{\psi}(s\omega_k) = (\frac{2\pi s}{\delta t})^{(\frac{1}{2})}\pi^{-\frac{1}{4}} H(\omega_k) e^{-\frac{(s\omega_k-\omega_0)^2}{2}} \tag{2}$$

where $H(\omega_k)$ is the Heaviside step function, ω_0 is selected equal to 6 to satisfy admissibility (Farge, 1992) and the angular frequency ω_k varies as:

$$\omega_k = \frac{2\pi k}{N\delta t} : k \leqq \frac{N}{2}, \qquad \omega_k = \frac{-2\pi k}{N\delta t} : k > \frac{N}{2}. \tag{3}$$

Expression (2) is normalised by the total energy so that:

$$\int_{-\infty}^{+\infty} |\hat{\psi}_0(\omega')|^2 d\omega' = 1. \tag{4}$$

The vertical flux of a scalar is obtained from the product of the real component of the vertical velocity wavelet and that of the scalar (Hudgins et al., 1993; Druilhet et al., 1994). A space-wavelength representation of this product is usually referred to as a cross-scalogram.

The cross-wavelet power spectrum for two series of variables x_n and y_n with $n = 1, \ldots, N$, is given by:

$$|W_n^{xy}(s)| = |W_n^x(s) W_n^{y*}(s)| \tag{5}$$

where $W_n^{y*}(s)$ is the complex conjugate of the y wavelet. Following Torrence and Compo (1998) and using (5), we have determined the wavelet-95% confidence interval, i.e., the probability for cross-wavelet power to fall in a specific scale-space interval. The test assumes a χ^2 distribution of (5) and although it is derived for stationary or homogeneous signals (Torrence and Compo, 1998), it allows one to select the portions of the wavelet which are statistically significant. The range of scales investigated has been selected to fall between the minimum and maximum resolvable scales. Prior to the analysis the data have been de-trended.

4.1. Wavelet analysis for June 12

The results of the wavelet analysis for the flight perpendicular to the coast at 300 and 480 m a.s.l. are given in Figures 8 and 10 respectively for the fluxes of temperature, moisture and ozone. On the x-axis of Figure 8 the physical space is presented in km. The black shade at the bottom of the figure is again the terrain elevation measured by the aircraft. On the y-axis, the length scale is shown ranging from 80 to 2000 m, where the latter value still falls in the cone of influence of the wavelet. The 95% confidence interval is superimposed on the cross-scalogram (black curves). This means that the contoured structures are highly reliable as far as the wavelet treatment and statistical tests are concerned. The palette gives the value of the flux normalised with the product of the standard deviation of the respective variables (for example, $w'\theta'{\sigma_w}^{-1}{\sigma_\theta}^{-1}$). The values of the standard deviations used are given in Table II.

The top frame shows the cross-scalogram of temperature flux. The first feature that can be noticed is that between 9 km and 13.2 km from point D, clear structures are visible corresponding to a negative kinematic heat flux. These are mainly located at scales around 500 m. From point D up to 9.6 km from it, the cross-scalogram clearly shows the presence of larger scale structures corresponding to a positive heat flux at scales ranging from 200 to 700 m.

An interpretation of the cross-scalogram can be as follows. As the aircraft goes from point C to point D, it moves from the BFL (Figure 4) to the TIBL, thus passing from a region of mere heat advection to the turbulent TIBL (see also Figure 7). Since the first region encountered shows the presence of negative heat flux, and it coincides with the location of sudden variation of $w'\theta'$ (corresponding to the vertical dashed line), we conclude that this portion of the leg represents the passage

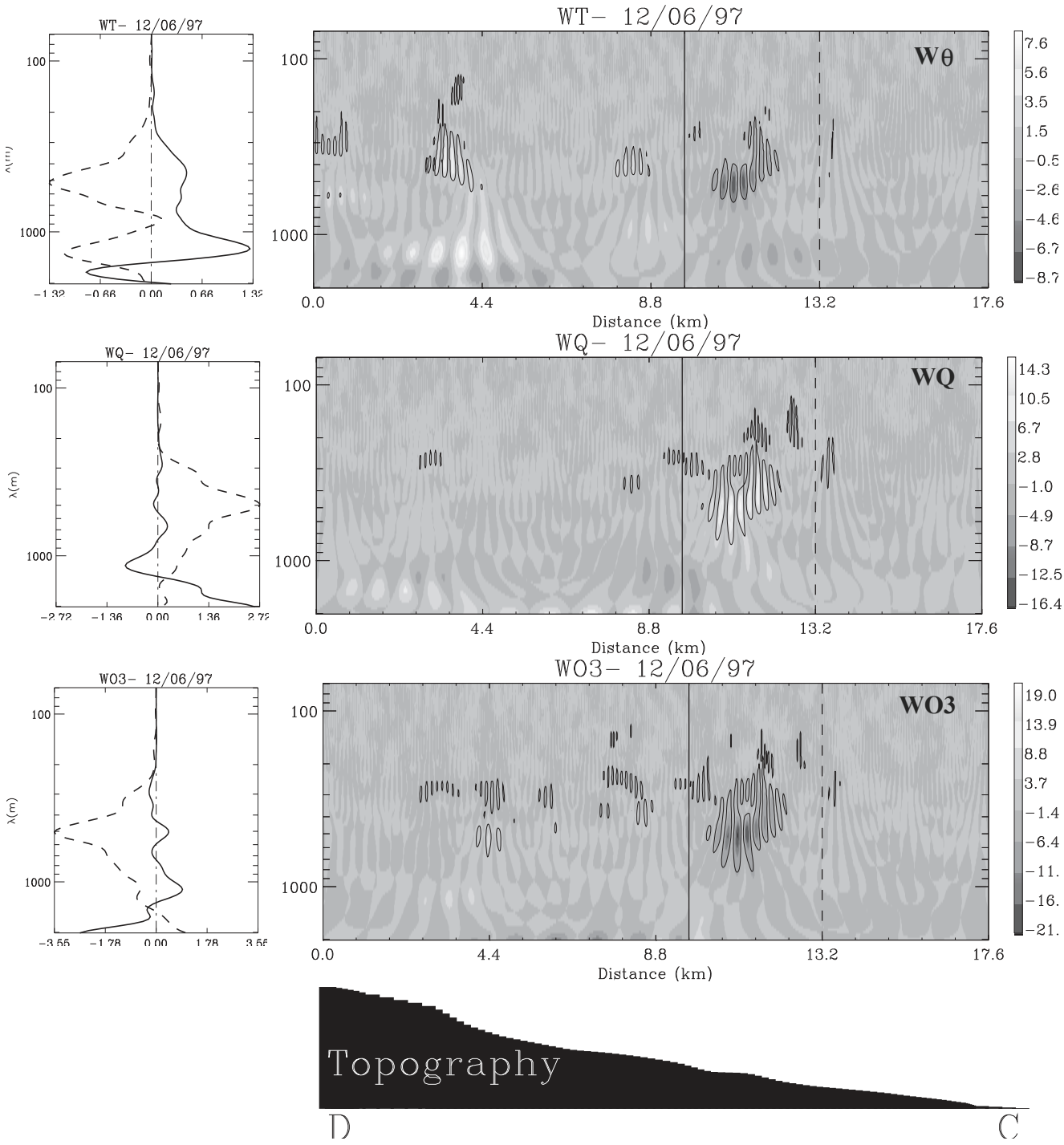

Figure 8. Cross-scalogram of $w'\theta'$ (upper panel), $w'q'$ (middle panel) and $w'O_3'$ (lower panel) for the 12 June flight at 300 m above sea level perpendicular to the coast. The palette gives the flux value normalised with standard deviations ($(x'y')(\sigma_x^{-1}\sigma_y^{-1})$). The black shade on the bottom represents the topography. The panels on the left represent the integrated scalograms of each flux. In particular: (dashed curve) integral between continuous vertical line and dashed vertical line of the scalogram; (thick curve) integral from point D to continuous vertical line of the scalogram.

through the TIBL-EZ. A partial confirmation of this hypothesis is given by the fact that as the aircraft proceeds towards point D, the measured heat flux is positive and distributed over larger scales (up to 700 m). This means that after having crossed the EZ, the leg proceeds through the bulk of the TIBL. A sharp variation of the flux sign and of the associated scales is clear from the picture (in correspondence to the

TABLE II

Values of the standard deviations with which the fluxes in Figures 8, 10 and 11 have been normalised.

	12-06 300 m (Figure 8)	12-06 480 m (Figure 10)	13-06 300 m (Figure 11)
σ_w (m s^{-1})	0.71	0.56	0.83
σ_θ (K)	0.27	0.56	0.33
σ_q (g kg^{-1})	0.77	0.45	0.95
σ_{O_3} (ppb)	3.1	3.11	6.23

vertical continuous line). The scales are here proportional to the TIBL depths and match well with the TIBL height determined from the temperature inversion.

The cross-scalograms of moisture and ozone fluxes shown in the other two frames of Figure 8, give further endorsement of the hypothesis made above. In the region identified as the TIBL-EZ (and enclosed by the two vertical lines), one can see structures with the same length scales as the heat flux, that give rise to a positive flux of moisture (as expected) and a negative flux of ozone (consistent with the presence of concentration maxima above the TIBL). For these two scalars the presence of larger-scale structures in the bulk of the layer is less evident than in the case of heat flux, but something still appears in the case of ozone at 4.4 km from D.

More precise information about the length scales involved in the turbulent transport process in the EZ can be determined by integrating the cross scalogram over a specific space range. The wavelet analysis shown in Figure 8 has therefore been integrated over the distance enclosed by the two vertical lines at 9.6 km and 13.2 km from D. Given the choice of the mother function, the result of the integration gives the co-spectrum of $w'\theta'$, $w'q'$ and $w'O_3'$ for the selected space range. The co-spectrum of the three fluxes is presented in the panels on the left of the scalograms of Figure 8. In the figure the dashed curve corresponds to the integration of the cross-scalogram enclosed between the continuous and the dashed vertical lines of Figure 8, whereas the continuous curve is the integration from D to the continuous vertical line, thus representing the cross-spectrum in the EZ and in the bulk of the TIBL, respectively. The cross-spectrum in the EZ shows the presence of a clear peak for the three scalar fluxes located at 500 m. The plots clearly show that the smallest scale present in the EZ is of the order of 300 m thus indicating that the turbulent fluxes at the TIBL top are governed by fairly large-scale structures or in other words by scales of the order of the TIBL depth in that space range. The peak in the $w'\theta'$ co-spectrum of the EZ at scales of the order of 1000 m is generated by wavelets excluded from the 95% confidence interval.

The wavelet analysis of the data collected at 480 m is presented in Figure 9. As shown in Figure 8, the three frames are the cross-scalograms of the fluxes of temperature, moisture and ozone. The frame next to each scalogram gives the integrated curves as in Figure 8. All the features evinced from the analysis of the flight at 300 m can be found also at 480 m, the only difference being that now the area that we have identified as the entrainment zone is approximately two kilometres wider. The scales appearing in the cross-spectra are at the same wavelength as those found at 300 m. Scales smaller than this order of magnitude do not contribute to the scalar vertical fluxes as it can be determined from the co-spectra. This is the case, for example of heat and moisture, for which statistically significant structures are visible in the cross-scalogram at a scale of 200–300 m although they do not contribute to the co-spectrum.

From the results of Figures 8 and 9 we can summarise the elements provided by the wavelet analysis that indicate the selected region is the EZ:

- in this region the fluxes of the three scalars have the characteristic EZ signs: negative for heat and ozone, and positive for moisture. In particular the localised negative heat flux is a clear indication of entrainment. The negative flux of ozone is due to the presence of concentration maxima above the TIBL so it is consistent with the actual situation;
- a dominant scale range is present in this region and is responsible for the turbulent transport process;
- the scales associated with the EZ are localised in space.

It is important to consider that, strictly speaking, an entrainment flux is given by the product of $w' < 0$ and $c' > 0$ where c' is the fluctuation of a generic scalar. The analysis made above gives clear indication that a zone of transition is indeed present between the TIBL and the BFL. What cannot be evinced from the cross-scalogram is whether the fluxes detected in this region, and in particular the heat flux, are pure entrainment fluxes or more generic fluxes at the top of the layer. We have therefore conducted a conditional sampling (Réchou and Durand, 1997) based on the signs of w' and θ'. The results are presented in Table III. At 300 m the dominant contribution to the entrainment flux is given by $w' < 0$ and $\theta' > 0$, which means that at this level the heat flux in the EZ is an entrainment flux. The same can not be said for the other two levels where the contribution to the total flux derives in almost the same proportion from positive ($w' > 0$, $\theta' > 0$ and $w' < 0$, $\theta' < 0$) and negative ($w' > 0$, $\theta' < 0$ and $w' < 0$, $\theta' > 0$) fluxes.

5. Wavelet Analysis for June 13

Figure 10 shows the wavelet analysis conducted on the data collected on the 13 June at noon at 300 m a.s.l. Differences and similarities from the flight at the same time and altitude presented in the previous section can be evinced.

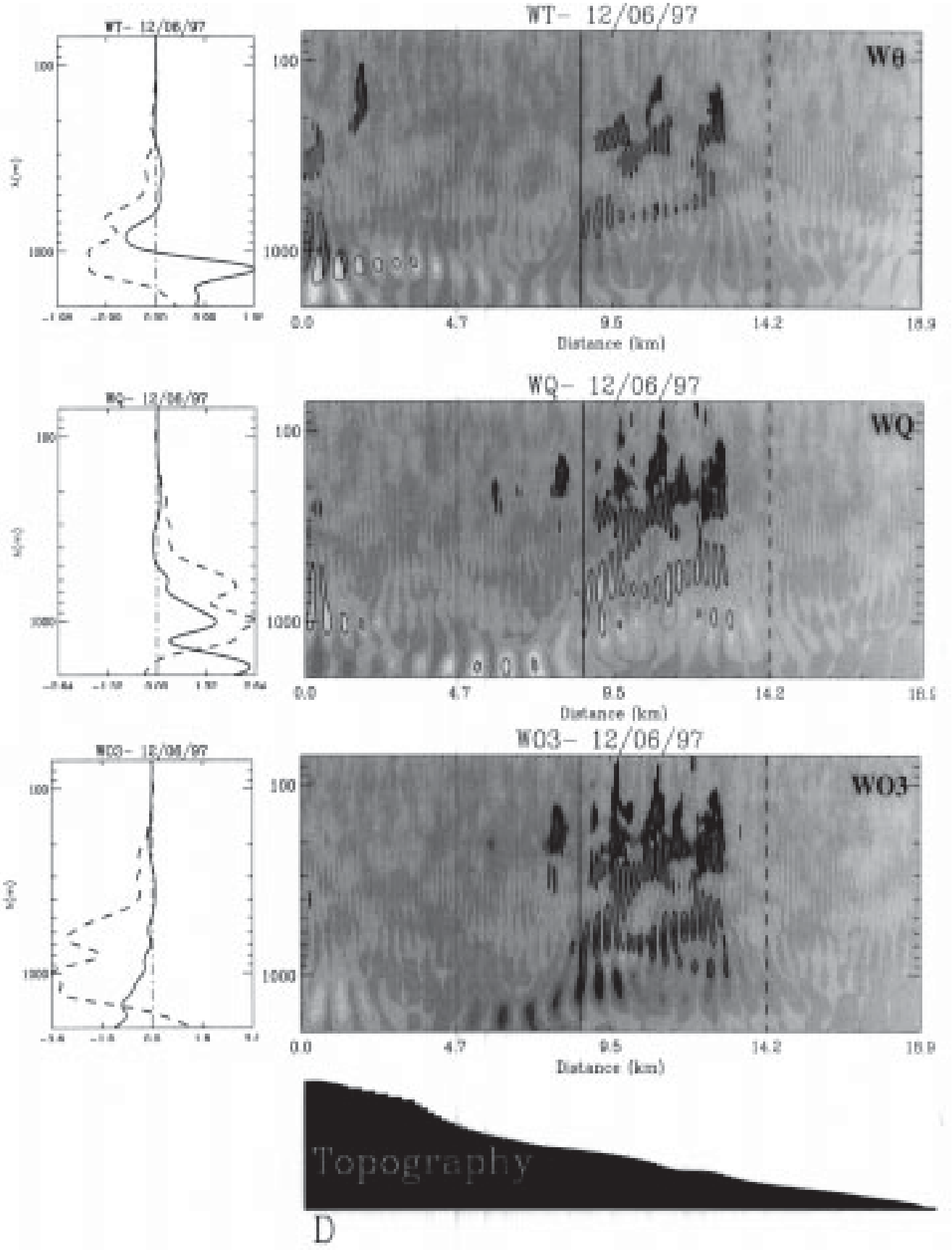

Figure 9. Same as Figure 8 for the 480 m leg.

TABLE III

Conditionally sampled kinematic heat flux (K m s^{-1}) in the EZ at the three measurement heights for 12 June.

	300 m	480 m	680 m
$w' > 0\, \theta' > 0$	0.0035	0.0102	0.0101
$w' > 0\, \theta' < 0$	−0.0089	−0.0282	−0.0251
$w' < 0\, \theta' > 0$	−0.0204	−0.0302	−0.0105
$w' < 0\, \theta' < 0$	0.0086	0.0151	0.0176

The first difference relates to the presence of a zone of negative and positive heat flux as the aircraft enters the TIBL. The scales detected by the wavelets are larger than those found for the same position in x and altitude for the previous day. At 14.2 km from point D other structures are present but they are not contoured by the 95% confidence curve. As the aircraft proceeds inland, wide updrafts are crossed and visible in the figure. These structures are characterised by a very large scale (1500 m) and can be considered reliable. To explain the origin of these large scales we can only hypothesise the presence of processes that are not associated with the TIBL dynamics. The moisture flux shows a structure more consistent with the results of the June 12 though the dominant scale is much larger (see dashed line on the left plot). No ozone flux is detected by the wavelet in the transition region from the BFL to the TIBL and in the bulk of the layer positive and negative fluxes can be seen. An interesting feature is the regular alternation of updrafts and downdrafts. In general the results of 13 June do not show the same consistency found for the previous day.

6. Entrainment to Surface Heat Flux Ratio

As shown in several studies concerning the convective boundary layer and the TIBL (e.g., Venkatram, 1977, 1986; Raynor et al., 1979; Druilhet et al., 1997; Hanna, 1987) a crucial parameter for the determination of the structural characteristics of the layer is the heat entrainment flux and how this compares with the surface flux. A widely used assumption is that as for the CBL, the ratio of entrainment to surface heat flux is 0.2. In this section we focus in particular on this ratio.

As mentioned earlier, one of the strong points of using wavelets to analyse data is that they provide fairly precise information on the spatial (temporal) location of a specific physical process. By means of the wavelet analysis we have determined a precise region of the TIBL that shows characteristics typical of the EZ. We are therefore in the position of estimating this ratio.

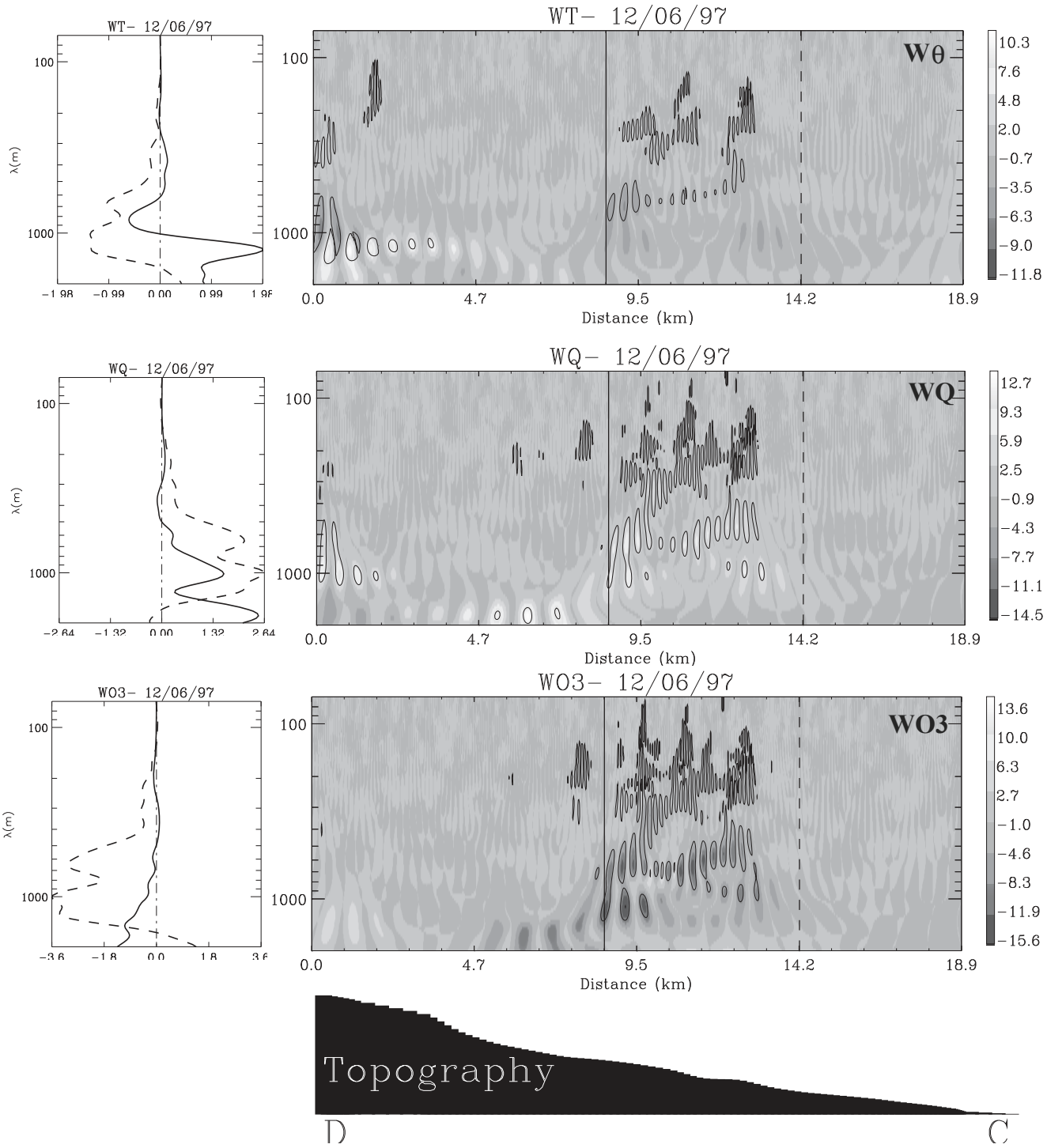

Figure 10. Same as Figure 9 for the 300 m leg on the 13 of June at noon.

An obstacle at this point is to obtain the surface value of the heat flux. We have estimated it by extrapolating the value from the measurements collected during the flights.

In Table IV the flux ratios are presented. The table shows the minimum and maximum of the absolute value of the flux ratio for all the available levels on 12 June. The procedure adopted to obtain the figures given in the table has been to: identify the entrainment zone from the cross-scalogram; extrapolate the surface values over the horizontal extent of the zone; estimate the ratio using the flux calculated in the identified entrainment zone. The results show a wide range of

TABLE IV

Absolute value of the ratio of the temperature flux in the EZ and surface value. The range gives the minimum and maximum value of the ratio. The second column gives the value of the parameter α that relates the TIBL height to the square-root of distance as from Venkatram (1986). The distances from the coast (d) have been retrieved from the cross scalogram.

	$\lvert(\overline{w'\theta'}_{EZ})(\overline{w'\theta'}_{0})^{-1}\rvert$	α	d (km)
680 m	0.07–0.12	2.2–2.8	14
480 m	0.39–0.7	6.3–3.5	8
300 m	0.15–0.27	1.41–3.0	7

values with a minimum ratio of 0.05 and a maximum of 0.7. Ratio values smaller or larger than 0.2 can be attributed to two reasons:

1. Despite the fact that the flux at the top of the TIBL has been calculated rather accurately, a degree of uncertainty is present in the surface flux value.
2. Extra contributions to the flux other than entrainment are present in the EZ and have been accounted for.

Given the result of the conditional sampling in the EZ presented in Section 4.1, the second explanation given above seems to be quite realistic. The results of Tables III and IV are in fact quite consistent since only at 300 m a value close to 0.2 is found and at the same level the entrainment flux was dominant.

The analysis conducted on 12 June could not be repeated for the 13th, given the difficulty of identifying precisely the EZ as described in the previous section. A similar analysis would introduce too many uncertainties to be reliable.

Using the formula suggested by Venkatram (1986) that relates linearly the TIBL height to the square-root of inland distance from the coast we have determined the proportionality constant α using the values presented in Table IV. Our results fall quite nicely in the range of variability deduced from other datasets presented by Hsu (1986).

7. Conclusions

The aircraft measurements collected during the *BEMA* campaign conducted on the east coast of Spain North of Valencia (Burriana) on June 1997 have been analysed. Attention has been focused on the mean and turbulent variables collected in a plane perpendicular to the coast line on two specific days (12 and 13 June) during which a clear sea-breeze regime was present.

The atmosphere over the sea and the coast shows a clearly layered structure in the vertical. Over the sea three layers can be identified. Between the sea breeze and the return flow, the presence of a rather shallow layer can be evinced in which the wind blows northward perpendicular to the return flow.

The turbulent and mean measurements collected over the coast clearly show the presence of a Thermal Internal Boundary Layer (TIBL) developing inland from the coast and extending in the vertical for approximately a thousand metres at the innermost location reached by the aircraft (20 km inland). The fields of kinematic and scalars covariances indicate the presence of a region located on the top of the TIBL, which is characterised by negative fluxes of temperature and ozone and positive fluxes of moisture. In the very same region the scalar variances show a maximum value typically found on the top of horizontally homogeneous convective boundary layers. All these elements indicate this region as the Entrainment Zone (EZ) of the TIBL.

In order to gather further evidence to substantiate this hypothesis and provide a more quantitative characterisation of this region, a wavelet analysis of the vertical fluxes of heat, moisture and ozone has been conducted. Using the classical Morlet mother function and the data collected at different altitudes above sea level in a plane perpendicular to the coast, the cross-scalograms of $w'\theta'$, $w'q'$ and $w'O_3'$ have been calculated. From the wavelet analysis the following conclusions have been reached:

- in the location in which the aircraft passes from the breeze layer to the TIBL, a region can be identified that shows characteristics not found in the rest of the layer;
- this region extends for approximately two kilometres in the horizontal;
- in this region the fluxes of the three scalars are positive for moisture and negative for ozone and heat;
- the scales characterising the fluxes in this region are smaller than those found in the bulk of the layer.

The same type of analysis conducted on 13 June allows us to draw similar conclusions though the results obtained do not show the same completeness and self consistency found on 12 June. As a matter of fact, we cannot expect to find the very same type of behaviour found on the 12th since the EZ and the TIBL are after all average structures or archetypes obtained on the basis of statistics larger than two cases.

Having identified a possible EZ by taking advantage of the wavelet capacity to confine physical properties in space, we have calculated the entrainment to surface heat flux ratio. The results give values that fall well within the range indicated in the literature. Values much larger and much smaller than 0.2 have also been found that can be attributed to a heat flux in the EZ that does not correspond to pure entrainment, as was shown from the conditional sampling analysis conducted on the EZ heat flux.

Future investigation will be aimed at collecting more information on the structural characteristics of the TIBL by using other turbulence parameters measured during the campaign. Subjects of interest will be the structure of the layer along the coast and the study of the transition region between the TIBL and the MBL. In both cases wavelet analysis is likely to be an adequate tool, associated with other techniques, for the study of these types of measurement.

Acknowledgements

The Biogenic Emission over the Mediterranean Area (*BEMA*) experiment was sponsored by the Commission of the European Union. We are grateful to Drs. P. Bechtold and P. Durand for their comments during the preparation of this manuscript and to Dr. J. Matthijsen for having fostered this collaboration.

References

Réchou, A. and Durand, P.: 1997, 'Conditional Sampling and Scale Analysis of the Marine Atmospheric Mixed Layer – SOFIA Experiment', *Boundary-Layer Meteorol.* **82**, 81–104.

Druilhet, A. and Durand, P.: 1997, 'Experimental Investigation of Atmospheric Boundary Layer Turbulence', *Atmos. Res.* **43**, 345–388.

Druilhet, A., Herrada, H., Pages, J. P., Daissat, J., Allet, Ch., and Ravaut, M.: 1997, 'Etude Expérimentale de la Couche Limite Interne Associée à la Brise de Mer', *Boundary-Layer Meteorol.* **22**, 511–608.

Druilhet, A., Attié, J. L., de Abreu Sá, L., Durand, P., and Bénech, B.: 1994, 'Experimental Study of Inhomogeneous Turbulence in the Lower Troposphere by Wavelet Analysis', in Charles K. Chui, Laura Montefusco, and Luigia Puccio (eds.), *Wavelet: Theory, Algorithms, and Applications*, Vol. 5. Academic Press, Inc., ISBN 0-12-174575-9.

Durand, P., Briere, S., and Druilhet, A.: 1989, 'A Sea-Land Transition Observed during the COAST Experiment', *J. Atmos. Sci.* **46**, 395–457.

Farge, M.: 1992, 'Wavelet Transforms and their Applications to Turbulence', *Annu. Rev. Fluid. Mech.* **24**, 395–457.

Garratt, J. R.: 1990, 'The Internal Boundary Layer – A Review', *Boundary-Layer Meteorol.* **50**, 171–203.

Garratt J. R.: 1992, *The Atmospheric Boundary Layer*, Cambridge Univ. Press, U.K., 316 pp.

Grossman, A. and Morlet, J.: 1984, 'Decomposition of Hardy Functions into Square Integrable Wavelets of Constant Shape', *J. Math. Anal.* **15**, 723–736.

Hanna, S.: 1987, 'An Empirical Formula for the Height of the Coastal Internal Boundary Layer', *Boundary-Layer Meteorol* **40**, 244–250.

Hudgins, L. H., Friche, C. A., and Mayer, M. E.: 1993, 'Wavelet Transform and Atmospheric Turbulence', *Phys. Rev. Lett.* **71**, 3279–3282.

Hsu, S.: 1986, 'A Note on Estimating the Height of the Convective Internal Boundary Layer near the Shore', *Boundary-Layer Meteorol.* **35**, 311–316.

Lambert, D. and Durand, P.: 1998, 'Aircraft to Aircraft Intercomparison during SEMAPHORE', *J. Geophys. Res.* **103**, 25109–25125.

Millan, M., Artinano, B., Alonso, L., Castro, M., Fernandez-Patier, R., and Goberna, J.: 1971, 'Mesometeorological Cycles of Air Pollution in the Iberian Peninsula', Technical Report, EV4V-0097-E, European Commission.

Ohara, T. and Ogawa, Y.: 1985, 'The Turbulent Structure of the Internal Boundary Layer near the Shore, Part II: Similarity and Energy Budgets Analysis', *Boundary-Layer Meteorol.* **32**, 39–56.
Oke, T. R.: 1987, *Boundary Layer Climates*. Methuen, New York, 435 pp.
Raynor, G. Michael, P., Brown, R., and Sethuraman, S.: 1975, 'Studies of Atmospheric Diffusion from a Nearshore Oceanic Site', *J. Appl. Meteorol.* **14**, 1080–1094.
Raynor, G., Sethuraman, S., and Brown, R.: 1979, 'Formation and Characteristics of Coastal Internal Boundary Layers during Onshore Flows', *Boundary-Layer Meteorol.* **16**, 487–514.
Seufert, G. (ed.): 1997, 'BEMA, A European Commission Project on Biogenic Emission in the Mediterranean Area', *Atmos. Environ.* **31**, 1–256.
Simpson, J.E., Mansfield, D. A., and Milford, J. R.: 1980, 'Inland Penetration of Sea-Breeze Fronts', *Quart. J. Roy. Meteorol. Soc.* **106**, 485–500.
Smedman, A.-S. and Hogstrom, U.: 1983, 'Turbulence Characteristics of a Shallow Convective Internal Boundary Layer', *Boundary-Layer Meteorol.* **25**, 271–287.
Steyn, D. G. and Oke, T. R.: 1982, 'The Depth of the Daytime Mixed Layer at Two Coastal Sites: A Model and its Validation', *Boundary-Layer Meteorol.* **24**, 161–180.
Stunder, M. and Sethuraman, S.: 1985, 'A Comparative Evaluation of the Coastal Internal Boundary Layer Development', *Boundary-Layer Meteorol.* **32**, 177–204.
Tennekes, H.: 1974, 'The Atmospheric Boundary Layer', *Physics Today* **27**, 52–63.
Torrence, C. and Compo, G. P.: 1998, 'A Practical Guide to Wavelet Analysis', *Bull. Amer. Meteorol. Soc.* **79**, 61–78.
van Dop H. R., Steenkist, S., and Nieuwstadt, F. T. M.: 1979, 'Revised Estimates of Continuous Shoreline Fumigation', *J. Appl. Meteorol.* **18**, 133–137.
Venkatram, A.: 1977, 'A Model of the Internal Boundary Layer Development', *Boundary-Layer Meteorol.* **36**, 419–437.
Venkatram, A.: 1986, 'An Examination of Methods to Estimate the Height of the Coastal Internal Boundary Layer', *Boundary-Layer Meteorol.* **36**, 149–156.
Vugts, H. F. and Businger, J. A.: 1977, 'Air Modification Due To a Step Change in Surface Temperature', *Boundary-Layer Meteorol.* **11**, 295–305.
Weisman, B.: 1976, 'On the Criteria for the Occurrence of Fumigation Inland from a Large Lake – A Reply', *Atmos. Environ.* **12**, 172–173.